Draft version February 18, 2016
Preprint typeset using LaTeX style emulateapj v. 5/2/11

arXiv:1602.05363v1 [astro-ph.GA] 17 Feb 2016

DISTRIBUTIONS OF QUASAR HOSTS ON THE GALAXY MAIN-SEQUENCE PLANE

Zhoujian Zhang[1, 2, 3], Yong Shi[1, 2, 4], George H. Rieke[5], Xiaoyang Xia[6], Yikang Wang[1, 2], Bingqing Sun[7], Linfeng Wan[1,2]

Draft version February 18, 2016

ABSTRACT

The relation between star formation rates and stellar masses, i.e. the galaxy main sequence, is a useful diagnostic of galaxy evolution. We present the distributions relative to the main sequence of 55 optically-selected PG and 12 near-IR-selected 2MASS quasars at $z \leq 0.5$. We estimate the quasar host stellar masses from *Hubble* Space Telescope or ground-based AO photometry, and the star formation rates through the mid-infrared aromatic features and far-IR photometry. We find that PG quasar hosts more or less follow the main sequence defined by normal star-forming galaxies while 2MASS quasar hosts lie systematically above the main sequence. PG and 2MASS quasars with higher nuclear luminosities seem to have higher specific SFRs (sSFRs), although there is a large scatter. No trends are seen between sSFRs and SMBH masses, Eddington ratios or even morphology types (ellipticals, spirals and mergers). Our results could be placed in an evolutionary scenario with quasars emerging during the transition from ULIRGs/mergers to ellipticals. However, combined with results at higher redshift, they suggest that quasars can be widely triggered in normal galaxies as long as they contain abundant gas and have ongoing star formation.

Subject headings: infrared: galaxies — galaxies: active — galaxies: starburst

1. INTRODUCTION

Super-massive black-holes (SMBHs) are now known to be integral components of galaxies. The tight correlation between SMBH masses and their host galaxy properties (e.g. Kormendy & Ho 2013), and the similar mass growth rates between SMBHs and galaxies with cosmic time (Mullaney et al. 2012), indicate coevolution between the two (Heckman & Best 2014). Quasi-stellar objects (QSOs), the manifestation of dramatic accretion onto SMBHs, are the key stage of SMBH growth and represent an important phase in the evolution of massive galaxies (Sanders et al. 1988; Hopkins et al. 2006). Probing the properties of quasar hosts, e.g. host morphology (Dunlop et al. 2003), color (Jahnke et al. 2004), interstellar medium (Xia et al. 2012; Petric et al. 2015) and star formation behavior (Shi et al. 2007, 2014; Xu et al. 2015a), is essential to understanding the environment where SMBHs grow, and to gain insights into the circumstances influencing coevolution.

Color-magnitude diagrams are frequently employed to investigate AGN host properties (Silverman et al. 2008; Xue et al. 2010). However, the colors and magnitudes of galaxies can be affected by extinction, metallicity, the age of the stellar populations, and star formation rates as well as by the stellar mass. On the other hand, the galaxy main sequence characterizes the relationship between star formation rates (SFRs) and stellar masses ($M_\star$) of normal star-forming galaxies (Brinchmann et al. 2004; Daddi et al. 2007). Elliptical galaxies lie about ~ 1.5 dex below the typical SFRs of main sequence galaxies at a given stellar mass, while starbursts are located significantly above ($\gtrsim 0.6$ dex) it (Whitaker et al. 2012). The redshift evolution of the main sequence shows the roles of increased gas content and more efficient star formation triggering mechanisms at high redshift (Whitaker et al. 2012). Therefore, the main sequence investigation that studies the locations of galaxies in the SFR vs. stellar mass plane, is less degenerate in physical interpretation than color-magnitude approaches.

Previous studies of AGN relative to the main sequence of galaxies mainly focus on deep survey data, and thus on the high-z regime (Xue et al. 2010; Mullaney et al. 2012; Harrison et al. 2012; Rosario et al. 2013; Xu et al. 2015a; Mullaney et al. 2015), or on moderate-luminosity AGN at low-z (e.g. Shimizu et al. 2015). Instead, we will quantify the distribution along the main sequence of the Palomar-Green (PG; Schmidt & Green 1983) and Two Micron All Sky Survey (2MASS; Cutri et al. 2001; Smith et al. 2002) archetypal low-redshift quasar samples. This study builds on that of Shi et al. (2014), who presented infrared spectroscopic and photometric observations of PG and 2MASS quasars and used them to derive star formation rates. We complement these results by estimating the stellar masses using the optical/near-IR photometric measurements of quasar hosts from the literature based on *Hubble* Space Telescope and ground-based adaptive optics (AO) observations.

2. SAMPLE

We drew sources for our study from the parent samples of 88 PG quasars at $z \leq 0.5$ and 63 2MASS quasars at $z \leq 0.4$. PG quasars are representative of bright

[1] School of Astronomy and Space Science, Nanjing University, Nanjing 210093, China
[2] Key Laboratory of Modern Astronomy and Astrophysics (Nanjing University), Ministry of Education, Nanjing 210093, China
[3] Current address: Institute for Astronomy, University of Hawaii, 2680 Woodlawn Drive, Honolulu, HI 96822, USA
[4] Collaborative Innovation Center of Modern Astronomy and Space Exploration, Nanjing 210093, China
[5] Department Of Astronomy And Steward Observatory, University of Arizona, 933 N Cherry Ave, Tucson, AZ 85721, USA
[6] Tianjin Astrophysics Center, Tianjin Normal University, Tianjin 300387, China
[7] National Astronomical Observatories, Chinese Academy of Sciences, Beijing 100012, China

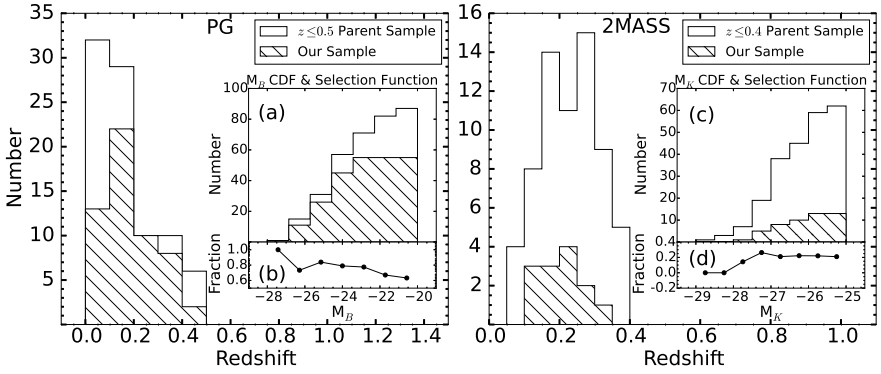

FIG. 1.— Redshift distributions of PG (*left*) and 2MASS (*right*) samples adopted in this study (*diagonal hatches*), as compared with the parent samples (*white area*). The subplots show the cumulative distribution of their absolute magnitudes (B-band for PG and K-band for 2MASS sample) and the selection function.

optically selected quasars and are all classified as type 1. 2MASS quasars represent a redder quasar population compared to PG quasars but have similar K_s-band luminosity (Smith et al. 2002). The 2MASS quasars contain a broad range of types including 21 type 1, 37 intermediate, 4 type 2 and 1 low-ionization emission line object.

To find objects suitable for determination of host galaxy masses, we searched the HST archive. Our final sample contains 56 PG objects at $z \leq 0.5$ and 13 2MASS objects at $z \leq 0.4$. 53 PG and all 2MASS sample have HST images, which we prefer due to the better PSF stability; we also include three PG objects which were observed only by the Gemini-N or the Subaru Telescope with AO (Guyon et al. 2006). Although we included only a small number of 2MASS objects, they are representative of the parent sample both in redshift and luminosity (Marble et al. 2003; Shi et al. 2014).

As shown in Figure 1, our sample contains $\sim 63\%$ of the PG and $\sim 20\%$ of the 2MASS parent sources. The inserted plots show that our PG and 2MASS quasars are biased toward the bright members of their parent samples; they are typically at $z \sim 0.16$ and $z \sim 0.21$ (median), respectively. For comparison, we also selected: a complete sample of 118 ULIRGs with ($f_{60\mu m} > 1$ Jy, Kim & Sanders 1998) at $z \sim 0.1$, plus 587, 673 SDSS galaxies (Brinchmann et al. 2004).

3. DERIVATION OF THE STELLAR MASS AND SFRS OF QUASAR HOSTS

The stellar masses of our quasar hosts are calculated from host galaxy absolute magnitudes reported in the literature. In all cases, these are based on decompositions of 2D images into host and nuclear components. The result is listed in Table 1. Note all literature measurements are rescaled to the cosmology at $H_0 = 70$ km s^{-1} Mpc^{-1}, $\Omega_M = 0.3$ and $\Omega_\lambda = 0.7$.

Before deriving stellar masses, we examine the consistency of the measurements from the seven studies we utilize. Overall, their methods used to remove the quasar contamination are very similar. The image was decomposed into the quasar and host light with a two-dimensional analysis, with a stellar image or TinyTim-produced PSF image representing the quasar contribution. The host component was usually represented by a single de Vaucouleurs (elliptical) and a single exponential (disk) model, although sometimes an additional de Vaucouleurs plus exponential (bulge+disk) were added. The final result was determined by χ^2 minimization. For the PG sample, Veilleux et al. (2009) confirmed that their HST measurements were in good agreement with the prior ground-based and HST ones from McLeod & McLeod (2001), Guyon et al. (2006), Hamilton et al. (2008), which contain $\sim 95\%$ of our sample (see their Figure 7). The only exception is that the AO measurements from Guyon et al. (2006) overestimate the host magnitudes by ~ 0.3 mag, which we corrected for sources from this study. Since the 2MASS host galaxies are typically brighter than their nuclei by ~ 0.3 mag, it is reasonable to believe the reliability of the decompositions.

We estimated the stellar masses as follows. First, an absolute luminosity was calculated from this magnitude. For the 46 PG quasars with H or K band data, the magnitude was converted to the luminosity at the band of the magnitude with no K-correction. The optical magnitudes of the remaining 10 PG and all 13 2MASS sources were converted into r-band and i-band luminosities with appropriate K-corrections, based on the SWIRE template library (Polletta et al. 2007). Given the lack of the optical color, we derived two K-corrections for each object corresponding to elliptical and spiral SED templates. We chose the elliptical template with an age of 5 Gyr and the Sb galaxy template for spirals. The different SEDs result in at most a 7% difference in derived mass. Second, stellar masses were estimated based on the luminosities. Xu et al. (2015b) demonstrate the accuracy of such single-band mass estimates compared with those from more complete photometry. For H- and K-band luminosities, we adopted the logarithmic stellar-mass/light ratio of - 0.017 and -0.08, respectively (Bell et al. 2003). For hosts with optical luminosities, since we do not have an optical color we derived two stellar masses using two mass-to-light ratios, one appropriate for blue galaxies and the other for elliptical galaxies. With the SDSS galaxies from the MPA/JHU catalog with stellar mass above 10^{10} $M_\odot$, we found the distribution of the mass-to-light ratios can be described by a combination of two Gaussians: $\log(M_\star/M_\odot) + M_\lambda/2.5 = 2.23\pm0.09$ for red and 1.99 ± 0.18 blue in r-band, and 2.1 ± 0.07 for red and 1.89 ± 0.15 for blue in i-band, where M_λ is the absolute magnitude in AB.

The final quoted errors are based on uncertainties in the host galaxy photometry and in the stellar M/L. For the first, we adopt the results from the works reporting the host photometry, since they performed detailed error analysis taking account of the residuals from PSF subtraction. For the M/L, we adopt the typical uncertainties in the NIR ($\sim$ 0.2 dex), and optical bands ($\sim$ 0.08 for ellipticals, and $\sim$ 0.17 dex for spirals from the SDSS galaxy distributions) to describe the scatter of the conversion. For nine PG quasars with dynamical measurements of host galaxies by Dasyra et al. (2007), we found that our photometric masses are lower than the dynamical masses by only a factor of 1.2 (median), indicating no large systematic offset in our mass estimates.

The SFRs were obtained from Shi et al. (2014). Basically, the aromatic features or 160 μm are used to estimate the SFRs based on the star-forming templates provided by Rieke et al. (2009). In cases where we have 70um photometry and at least one of (i) aromatic features or (ii) 160um photometry, we use the latter to calibrate the relationship between 70um photometry and SFR. We then use this relationship to calculate SFRs in cases where we only have 70um photometry. The SFR estimates of the sample in this paper are the following: (1) 11.3 μm aromatic features (1 object); (2) MIPS 70 μm photometry (18 objects); and (3) MIPS or PACS 160 μm photometry (48 objects). However, the weak host galaxy infrared emission from PG2349-014 and 2MASS J023430.6+243835 made it hard to estimate their SFRs, so we eliminated them from subsequent analysis.

4. RESULTS

4.1. *Distribution of quasars along the main sequence*

The distribution of our 67 quasar host galaxies in SFR vs. stellar mass is shown in Figure 2 with the 1 Jy ULIRGs and SDSS DR7 galaxies (see Section 2) overlaid. The stellar masses of the 1 Jy ULIRGs are from their K$'$ band magnitudes (Kim et al. 2002) as discussed in Section 3, and their SFRs are estimated from the far-infrared luminosities (Kim & Sanders 1998) based on the scaling relation by Kennicutt (1998). The SFRs and stellar masses of the SDSS galaxies are from the SDSS MPA/JHU catalog, multiplied by 1.5 to convert to the Salpeter IMF. We used the quantitative fitting of SDSS galaxies from Peng et al. (2010) adjusted to the Salpeter IMF to define the main sequence. The upward and downward boundaries are set to be $\pm$ 0.6 dex, which is twice the 1-σ scatter of the main sequence (Daddi et al. 2007). The dividing line between the "green valley" and red galaxies is estimated by eye, roughly 1.0 dex below the main sequence.

As shown in Figure 2, the majority of PG quasar hosts reside within the main sequence, with 23% in the starburst regime and 11% in the green valley. The median distance of these galaxies to the main sequence is small, only 0.07 dex. The standard deviation of these distances is about 0.41 dex. Although this is larger than the 1-σ scatter (0.3 dex) of the main sequence itself, the large measured errors of the specific SFRs of the PG quasar hosts could broaden the intrinsic scatter. PG quasar host galaxies thus seem to follow more or less the main sequence.

2MASS quasar host galaxies, on the other hand, systematically lie above the main sequence, with only 1 out of 12 objects below. The median distance of 2MASS quasar hosts to the main sequence is 0.43 dex with a standard deviation of 0.33 dex. Super-giants in starbursts can contribute to the NIR bands (Shier et al. 1996), possibly making the NIR-selected 2MASS sources biased toward ones with higher SFRs.

4.2. *sSFR of quasar hosts as a function of global SMBH and host properties*

We here investigate the specific SFR (sSFR = SFR/M$_\star$) of quasar hosts as functions of global SMBH and host properties. SMBH masses are extracted from Veilleux et al. (2009) by averaging the results from different methods, including spheroid luminosity, spheroid velocity dispersion, reverberation mapping, and virial relation. A bolometric correction from Elvis et al. (1994) was assumed for Eddington ratios. As shown in Figure 3 (a), despite the large scatter, higher nuclear luminosity quasars seem to have on average higher sSFRs, e.g., at $M_{\rm B} <$ -25 the majority of PG quasars lie above the sequence with the median 0.42 dex higher than the sequence, while lower B-band luminosity PG quasars distribute around the main sequence with a median value 0.11 dex below the sequence. A recent work by Shimizu et al. (2015) points out that the distribution of moderate-luminosity AGN at low-z peaks $\sim$ 0.6 dex below the main sequence. It seems that their result represents an extension of our finding of higher SFRs in higher nuclear luminosity AGN hosts. Figure 3 (b) shows no relationship with morphologies (elliptical, spirals and merging). sSFRs are neither apparently enhanced in major mergers nor suppressed in elliptical hosts. No relationships are seen with SMBH masses or Eddington ratio as shown in Figure 3 (c) and Figure 3 (d), respectively.

4.3. *Redshift evolution of the sSFR of quasar hosts*

Figure 4 shows the redshift evolution of the sSFRs of our quasar hosts along with those of IR-selected high-z quasars from Xu et al. (2015a), providing further evidence that the PG quasar hosts follow more or less the evolution of the main sequence. At z = 0.3-0.5, PG quasar hosts have some bias toward higher sSFRs, in contrast to those below z = 0.3. At similar redshifts (0.3-0.5), quasars from Xu et al. (2015a) have lower luminosities than ours but show lower SFRs. This suggests that it is the luminosity instead of the redshift that causes PG quasar hosts to tend to have higher sSFRs at z = 0.3-0.5.

5. DISCUSSION: COMPARISONS WITH OTHER STUDIES

Xu et al. (2015a) investigated SFRs and stellar masses of 24μm-selected quasars up to z = 1.8. For about half of their sample, SFRs can be measured based on individual detections in the far-IR. As with our study, their sample is composed of high-luminosity AGN, i.e. quasars, and has enough objects ($\sim$ 300) to reach statistically robust conclusions. They found that the quasar hosts roughly follow the main sequence to z = 1.8.

Xue et al. (2010) compared color and SFRs of moderate luminosity X-ray, narrow-line AGN hosts to galaxies of similar stellar mass but without AGN, and found at z >1 that the two stellar-matched-mass samples have similar SFRs. However, below z=1 they found 2-3 times

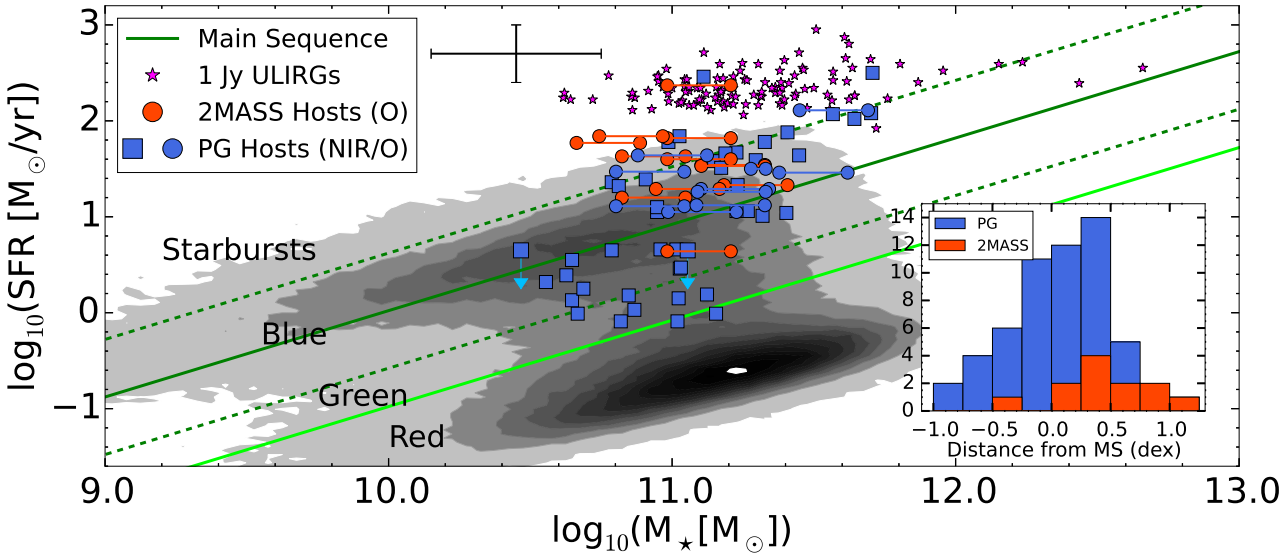

FIG. 2.— SFR–$M_\star$ relation for 67 2MASS (*red*) and PG (*blue*) quasar hosts. Galaxies with NIR measurements appear as squares, while those with optical photometry are shown as two circles corresponding to two K-corrections (see text). The typical error-bar is also noted. Over-plotted data include 118 complete 1 Jy ULIRGs (*pink stars*) and 587,673 SDSS DR7 galaxies (*filled grey contours*). Contours in grey scale show the number density of the SDSS sample, and demonstrate a bimodal distribution. The *dark green solid line* describes the main sequence (Peng et al. 2010) with two dashed lines 0.6 dex above and below the sequence; the *lime solid line* is visually determined as the boundary between green valley and red galaxies, that is about 10 times below the sequence. In addition, two light blue *downward arrows* are for PG 0026+129 and PG1121+422, whose SFRs are 3σ values. The subplot at the right lower corner shows the distributions of the distance of our 2MASS (red) and PG (blue) objects to the main sequence.

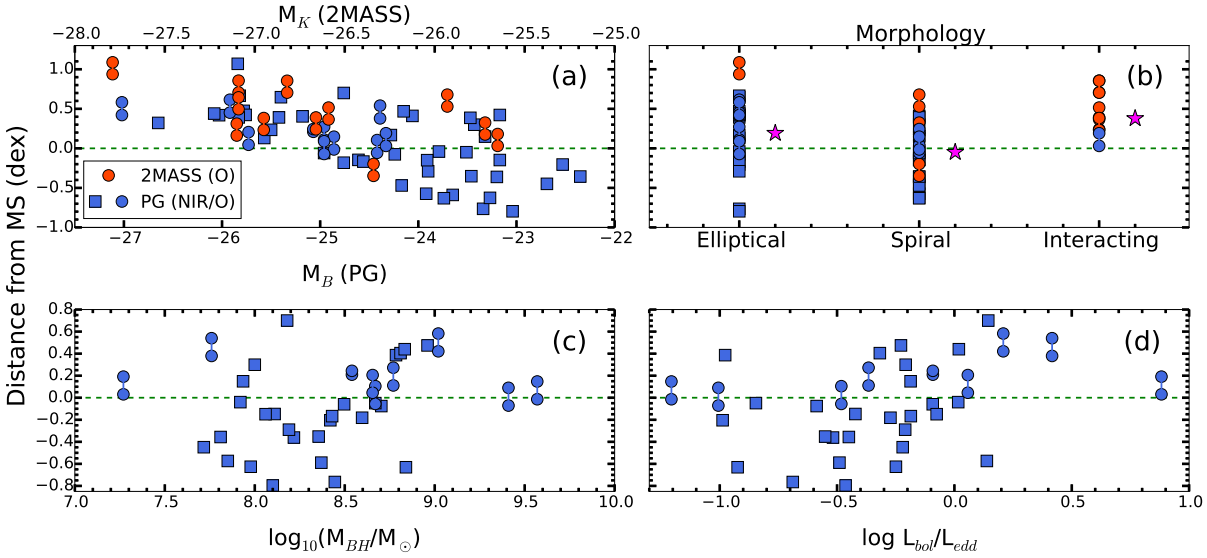

FIG. 3.— Distance to the MS as a function of (a) nuclear luminosities for PG (with NIR/optical photometry) at B-band and 2MASS (optical) at K-band, (b) morphology types, (c) SMBH masses for PG quasars and (d) Eddington ratios for PG quasars.

higher SFRs for the galaxies with AGN. Nonetheless, as shown in Figure 4, the host galaxies in their sample tend to fall on or below the main sequence, with a minority in the starburst regime, including those at z < 1. Mullaney et al. (2012) used *Herschel* 100 and 160 μm measurements to investigate the SFRs of moderate luminosity X-ray AGN ($L_{\rm x}$=10^{42-44} erg/s) at z = 0.5-3. Their color selection to identify cases where the stellar output is dominant (allowing accurate host mass estimates) strongly favors type 2 AGN, so their final sample resembles that of Xue et al. (2010). Based on the individually detected far-IR sources combined with a stacking analysis, they found that the SFRs of these AGN hosts roughly follow the main sequence with slightly lower (20%) average SFR values. This combined with their findings of no relationship between SFRs and SMBH accretion rates support their suggestion that moderately luminous AGN are unlikely to be triggered by major mergers instead of internal processes, and that there may be no causal link between nuclear activity and

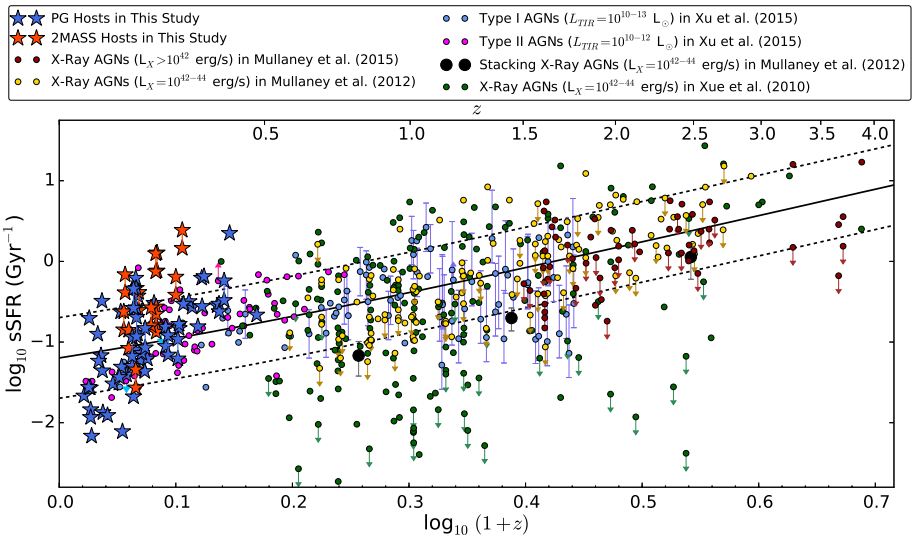
PG Hosts in This Study
2MASS Hosts in This Study
X-Ray AGNs (L$_X$>10^{42} erg/s) in Mullaney et al. (2015)
X-Ray AGNs (L$_X$=10$^{42-44}$ erg/s) in Mullaney et al. (2012)
Type I AGNs (L_{TIR}=10$^{10-13}$ L$_\odot$) in Xu et al. (2015)
Type II AGNs (L_{TIR}=10$^{10-12}$ L$_\odot$) in Xu et al. (2015)
Stacking X-Ray AGNs (L$_X$=10$^{42-44}$ erg/s) in Mullaney et al. (2012)
X-Ray AGNs (L$_X$=10$^{42-44}$ erg/s) in Xue et al. (2010)
z
log$_{10}$ sSFR (Gyr^{-1})
log$_{10}$ (1+z)

FIG. 4.— Redshift evolution of sSFRs of our quasar hosts along with measurements from the literature.

star formation. Harrison et al. (2012) investigated X-ray-luminous AGN ($L_{\rm x} > 10^{44}$ erg/s) and found their average SFRs are not suppressed or enhanced compared to star-forming galaxies at the same redshift. A similar result is found for optically-selected and X-ray-selected quasars between z=0.5 and z=2, again based on a stacking analysis (Rosario et al. 2013). By decomposing the SED including upper-limits to measured SFRs for individual X-ray sources at z=0.2-2.5, Stanley et al. (2015) reach similar conclusions.

The above studies based on deep surveys consistently found that the more luminous hosts of AGN follow more or less the main sequence of star-forming galaxies. However, for purely star-forming galaxies of similar mass ($> 10^{10} M_\odot$), the MS is a rough upper limit for the SFR and many galaxies fall well below it (Brinchmann et al. 2004). Similarly, AGN studies that measure the SFR individually in a substantial fraction of the observed sample find that the stacked results for the remainder also fall substantially below the MS (e.g., Xu et al. 2015b). Studies that rely more heavily on stacking may miss this behavior. In confirmation, Mullaney et al. (2015) observed some of their X-ray AGN hosts with ALMA and found a median SFR that is 0.4 dex below the main sequence. This result is similar to the low-redshift moderate-luminosity AGN that systematically lie below the sequence (Shimizu et al. 2015). The overall result is that AGNs of moderate and high luminosity reside in host galaxies that are not dramatically different from star-forming galaxies in general, and major mergers may not be the main mechanism to trigger star formation in AGN hosts.

We can also place our finding in the widely adopted picture of major-mergers driving both star formation and AGN (Sanders et al. 1988; Hopkins et al. 2006), as it is consistent with the evolutionary sequence from ULIRGs to type-2 quasars to type-1 quasars to elliptical in which sSFRs decrease from ULIRGs to obscured quasars (2MASS) to unobscured quasars (PG) to red dead ellipticals. However, the fact that PG quasars lie on the main sequence could also indicate that the triggering of quasars can happen widely in all types of galaxies with cold gas and ongoing star formation. Even in major mergers, the phase with enhanced SFRs is only a fraction of the whole duration of the interaction (Di Matteo et al. 2005), and quasars may be triggered in all phases of major mergers, which is consistent with no observed relationship between sSFRs and morphology types as seen in Figure 3 (b).

6. CONCLUSIONS

In summary, from the distribution of quasar hosts on the main-sequence plane, we found that PG quasars follow more or less the main sequence. Our small sample of 2MASS quasar hosts lies systematically above the sequence, a result possibly affected by a selection bias. The behavior of the PG quasars at z < 0.5 is similar to that for samples studied by others at z > 0.5. While no apparent relationships are observed between sSFRs and black-hole masses, Eddington ratio or even morphology types, quasars with higher nuclear luminosities show on average higher sSFRs despite a larger scatter. Although our finding is consistent with the merger-driven AGN scenario that links ULIRGs to type-2 quasars to type-1 quasars to ellipticals, it may also imply that quasars can be widely triggered in host galaxies with rich gas and ongoing star formation, without a close connection to major mergers.

We thank the anonymous referee for constructive comments that improve the paper significantly. Z.Z. and Y.S. acknowledge support for this work from the National Natural Science Foundation of China (grant 11373021), the Strategic Priority Research Program The Emergence of Cosmological Structures of the Chinese Academy of Sciences (grant No. XDB09000000), and Excellent Youth Foundation of Jiangsu Scientific Committee (grant BK20150014). Z.Z. also thanks for the support by the NSFC grant J1210039.

REFERENCES

Abazajian, K. N., Adelman-McCarthy, J. K., AgüEco's, M. A., PET AA. 2009, ApJS, 182, 543

Baldry, I. K., Glazebrook, K., Brinkmann, J., et val. 2004, ApJ, 600, 681

Bell, E. F., McIntosh, D. H., Futz, N., & Weinberg, M. D. 2003, ApJS, 149, 289
Brinchmann, J., Charlot, S., White, S. D. M., et al. 2004, MNRAS, 351, 1151
Bruzual, G., & Charlot, S. 2003, MNRAS, 344, 1000
Cutri, R. M., Nelson, B. O., Kirkpatrick, J. D., Huchra, J. P., & Smith, P. S. 2001, The New Era of Wide Field Astronomy, 232, 78
Daddi, E., Dickinson, M., Morrison, G., et al. 2007, ApJ, 670, 156
Dasyra, K. M., Tacconi, L. J., Davies, R. I., et al. 2007, ApJ, 657, 102
Di Matteo, T., Springel, V., & Hernquist, L. 2005, Nature, 433, 604
Dunlop, J. S., McLure, R. J., Kukula, M. J., et al. 2003, MNRAS, 340, 1095
Elvis, M., Wilkes, B. J., McDowell, J. C., et al. 1994, ApJS, 95, 1
Guyon, O., Sanders, D. B., & Stockton, A. 2006, ApJS, 166, 89
Hamilton, T. S., Casertano, S., & Turnshek, D. A. 2008, ApJ, 678, 22
Hamilton, T. S., Casertano, S., & Turnshek, D. A. 2002, ApJ, 576, 61
Harrison, C. M., Alexander, D. M., Mullaney, J. R., et al. 2012, ApJ, 760, L15
Heckman, T. M., & Best, P. N. 2014, ARA&A, 52, 589
Hopkins, P. F., Hernquist, L., Cox, T. J., et al. 2006, ApJS, 163, 1
Jahnke, K., Sánchez, S. F., Wisotzki, L., et al. 2004, ApJ, 614, 568
Kennicutt, R. C., Jr. 1998, ApJ, 498, 541
Kim, D.-C., & Sanders, D. B. 1998, ApJS, 119, 41
Kim, D.-C., Veilleux, S., & Sanders, D. B. 2002, ApJS, 143, 277
Kormendy, J., & Ho, L. C. 2013, ARA&A, 51, 511
Krist, J. E., Hook, R. N., & Stoehr, F. 2011, Proc. SPIE, 8127, 81270J
Marble, A. R., Hines, D. C., Schmidt, G. D., et al. 2003, ApJ, 590, 707
McLeod, K. K., & McLeod, B. A. 2001, ApJ, 546, 782
Mullaney, J. R., Pannella, M., Daddi, E., et al. 2012, MNRAS, 419, 95
Mullaney, J. R., Alexander, D. M., Aird, J., et al. 2015, MNRAS, 453, L83
Polletta, M., Tajer, M., Maraschi, L., et al. 2007, ApJ, 663, 81
Peng, C. Y., Ho, L. C., Impey, C. D., & Rix, H.-W. 2002, AJ, 124, 266
Peng, Y.-j., Lilly, S. J., Kovač, K., et al. 2010, ApJ, 721, 193
Petric, A. O., Ho, L. C., Flagey, N. J. M., & Scoville, N. Z. 2015, ApJS, 219, 22
Rieke, G. H., Alonso-Herrero, A., Weiner, B. J., et al. 2009, ApJ, 692, 556
Rosario, D. J., Santini, P., Lutz, D., et al. 2013, ApJ, 771, 63
Sanders, D. B., Soifer, B. T., Elias, J. H., et al. 1988, ApJ, 325, 74
Schmidt, M., & Green, R. F. 1983, ApJ, 269, 352
Sersic, J. L. 1968, Cordoba, Argentina: Observatorio Astronomico.
Shang, Z., Brotherton, M. S., Wills, B. J., et al. 2011, ApJS, 196, 2
Shi, Y., Ogle, P., Rieke, G. H., et al. 2007, ApJ, 669, 841
Shi, Y., Rieke, G. H., Ogle, P. M., Su, K. Y. L., & Balog, Z. 2014, ApJS, 214, 23
Shier, L. M., Rieke, M. J., & Rieke, G. H. 1996, ApJ, 470, 222
Shimizu, T. T., Mushotzky, R. F., Meléndez, M., Koss, M., & Rosario, D. J. 2015, MNRAS, 452, 1841
Silverman, J. D., Mainieri, V., Lehmer, B. D., et al. 2008, ApJ, 675, 1025
Smith, P. S., Schmidt, G. D., Hines, D. C., Cutri, R. M., & Nelson, B. O. 2002, ApJ, 569, 23
Stanley, F., Harrison, C. M., Alexander, D. M., et al. 2015, MNRAS, 453, 591
Veilleux, S., Kim, D.-C., Rupke, D. S. N., et al. 2009, ApJ, 701, 587
Whitaker, K. E., van Dokkum, P. G., Brammer, G., & Franx, M. 2012, ApJ, 754, L29
Xia, X. Y., Gao, Y., Hao, C.-N., et al. 2012, ApJ, 750, 92
Xu, L., Rieke, G. H., Egami, E., et al. 2015a, ApJ, 808, 159
Xu, L., Rieke, G. H., Egami, E., et al. 2015b, ApJS, 219, 18
Xue, Y. Q., Brandt, W. N., Luo, B., et al. 2010, ApJ, 720, 368

TABLE 1
PHOTOMETRY, STELLAR MASSES AND SFRS OF PG & 2MASS SAMPLE

Name (1)	z (2)	Morp. (3)	Inst. (4)	Band (5)	$M_{\rm host}$ (6)	$M_{\rm nuc}$ (7)	$m_{\rm total}$ (8)	host fraction (9)	$\sigma_{\rm host}$ (10)	R_e (kpc) (11)	Ref. (12)	log M$_\star$ ($M_\odot$) (13)	log SFR ($M_\odot$ yr^{-1}) (14)
PG 0007+106	0.089	E	NICMOS	H	-24.26	-24.58	...	...	0.07	2.97	5	11.02	0.66
PG 0026+129	0.142	E	NICMOS	H	-24.36	-25.82	...	...	0.22	0.90	5	11.06	<0.65
PG 0043+039	0.385	E	WFPC2	V	-21.94	-24.76	...	...	0.20	...	2, 4	[10.88, 11.12]	1.64
PG 0050+124	0.061	B+D	NICMOS	H	-24.96	-25.08	...	...	0.01	1.03	5	11.30	1.59
PG 0052+251	0.155	S	WFPC2	V	-22.35	-23.07	...	...	0.20	...	2, 4	[10.99, 11.23]	1.05
PG 0157+001	0.163	S	WFPC2	V	-23.61	-22.57	...	...	0.20	...	2, 4	11.71	2.50
		E	NICMOS	H	-25.99	-25.76	...	...	0.20	1.82	5		
PG 0804+761	0.100	Dp	⋆	H	-23.77	-26.09	...	...	0.26	...	7	10.82	-0.09
PG 0838+770	0.131	B+D	NICMOS	H	-25.02	-23.95	...	...	0.03	0.56	5	11.32	1.01
PG 0844+349	0.064	B+D	NICMOS	H	-23.89	-24.32	...	...	0.02	0.28	5	10.87	0.03
PG 0923+201	0.190	E	WFPC2	V	-22.27	-24.00	...	...	0.20		2, 4	11.27	1.06
		E	NICMOS	H	-24.89	-26.20	...	...	0.14	1.30	5		
PG 0947+396	0.206	D	NICMOS	H	-23.99	-25.69	...	...	0.12	...	1	10.91	1.39
PG 0953+414	0.234	S	WFPC2	V	-22.49	-24.50	...	...	0.20	...	2, 4	[11.10, 11.34]	1.29
PG 1001+054	0.161	E	NICMOS	H	-23.64	-25.27	...	...	0.18	2.38	5	10.65	0.55
PG 1004+130	0.240	S	WFPC2	V	-23.33	-24.89	...	...	0.20	...	2, 4	[11.38, 11.62]	1.46
PG 1012+008	0.185	S, I	WFPC2	V	-22.46	-23.02	...	...	0.20	...	2, 4	[11.09, 11.33]	1.26
PG 1048+342	0.167	E	NICMOS	H	-24.09	-24.29	...	...	0.22	...	1	10.95	1.05
PG 1100+772	0.315	...	NICMOS	J	...	...	14.45	0.270	0.22	...	6	11.45	1.64
		...	NICMOS	H	...	...	13.75	0.223	0.22	...	6		
		...	NICMOS	K	...	...	12.96	0.180	0.22	...	6		
PG 1116+215	0.177	S	WFPC2	V	-22.69	-24.46	...	...	0.20	...	2, 4	10.79	0.65
	0.176	?	NICMOS	H	-23.99	-27.31	...	...	0.51	...	5		
PG 1119+120	0.050	B+D	NICMOS	H	-23.84	-23.49	...	...	0.02	0.45	5	10.85	0.18
PG 1121+422	0.224	E	NICMOS	H	-22.89	-25.69	...	...	0.22	...	1	10.47	¡0.65
PG 1126–041	0.060	B+D	NICMOS	H	-24.30	-24.94	...	...	0.09	...	5	11.03	0.47
PG 1151+117	0.176	D	NICMOS	H	-23.29	-25.09	...	...	0.12	...	1	10.63	0.39
PG 1202+281	0.165	E	WFPC2	V	-21.89	-22.30	...	...	0.20	...	2, 4	[10.80, 11.04]	1.11
PG 1211+143	0.081	...	⋆	H	-23.11	-25.48	...	...	0.28	...	7	10.56	0.32
PG 1216+069	0.331	E	WFPC2	V	-21.82	-25.03	...	...	0.20	...	2, 4	11.03	1.84
		...	NICMOS	J	...	...	14.51	0.100	0.22	...	6		
		...	NICMOS	H	...	...	13.92	0.090	0.22	...	6		
		...	NICMOS	K	...	...	13.43	0.100	0.22	...	6		
PG 1226+023	0.158	E	WFPC2	V	-23.51	-26.46	...	...	0.20	...	2, 4	[11.45, 11.69]	2.11
PG 1229+204	0.064	S	WFPC2	V	-21.60	-21.54	...	...	0.20	...	2, 4	11.12	0.19
		B+D	NICMOS	H	-24.53	-23.71	...	...	0.10	3.65	5		
PG 1259+593	0.477	...	NICMOS	J	...	...	14.77	0.080	0.22	...	6	11.17	1.51
		...	NICMOS	H	...	...	13.88	0.064	0.22	...	6		
		...	NICMOS	K	...	...	13.04	0.050	0.22	...	6		
PG 1302–102	0.278	?	NICMOS	H	-25.24	-26.81	...	...	0.01	...	5	11.41	1.88
PG 1307+085	0.155	E	WFPC2	V	-21.69	-23.60	...	...	0.20	...	2, 4	10.96	0.66
		E	NICMOS	H	-24.12	-25.37	...	...	0.17	1.32	5		
PG 1309+355	0.184	S	WFPC2	V	-22.89	-23.80	...	...	0.20	...	2, 4	11.40	1.04
		E	NICMOS	H	-25.53	-25.89	...	...	0.06	3.49	5		
PG 1322+659	0.168	E	NICMOS	H	-23.69	-25.29	...	...	0.22	...	1	10.79	1.36
PG 1351+640	0.088	?	⋆	K′	-23.94	-25.99	...	...	0.28	...	7	10.81	1.32
PG 1352+183	0.158	D	NICMOS	H	-23.39	-24.59	...	...	0.12	...	1	10.67	-0.01
PG 1354+213	0.300	E	NICMOS	H	-24.59	-25.29	...	...	0.22	...	1	11.15	1.58
PG 1402+261	0.164	...	WFPC2	V	-21.89	-23.39	...	...	0.20	...	2, 4	[10.80, 11.04]	1.47
PG 1411+442	0.090	?	NICMOS	H	-24.28	-25.30	...	...	0.07	...	5	11.02	0.15
PG 1425+267	0.366	E	WFPC2	V	-22.72	-24.76	...	...	0.20	...	2, 4	11.33	1.78
		...	NICMOS	J	...	...	15.11	0.280	0.22	...	6		
		...	NICMOS	H	...	...	14.30	0.214	0.22	...	6		
		...	NICMOS	K	...	...	13.54	0.180	0.22	...	6		
PG 1426+015	0.086	S	WFPC2	V	-22.44	-23.14	...	...	0.20	...	2, 4	11.23	1.06
		B+D	NICMOS	H	-24.79	-24.98	...	...	0.06	1.64	5		
PG 1427+480	0.221	D	NICMOS	H	-24.09	-25.19	...	...	0.22	...	1	10.95	1.10
PG 1435–067	0.126	E	NICMOS	H	-23.44	-24.74	...	...	0.02	...	5	10.69	0.25
PG 1440+356	0.079	B+D	NICMOS	H	-24.80	-25.27	...	...	0.01	0.39	5	11.23	1.33
PG 1444+407	0.267	S	WFPC2	V	-23.08	-24.41	...	...	0.20	...	2, 4	[11.28, 11.33]	1.50
PG 1512+370	0.371	E	WFPC2	V	-22.93	-24.65	...	...	0.20	...	2, 4	11.19	1.66
		...	NICMOS	J	...	...	15.48	0.290	0.22	...	6		
		...	NICMOS	H	...	...	14.68	0.224	0.22	...	6		
		...	NICMOS	K	...	...	13.57	0.130	0.22	...	6		
PG 1543+489	0.400	...	NICMOS	J	...	...	15.12	0.150	0.22	...	6	11.11	2.46
		...	NICMOS	H	...	...	14.17	0.105	0.22	...	6		
		...	NICMOS	K	...	...	13.11	0.060	0.22	...	6		
PG 1545+210	0.264	E	WFPC2	V	-22.60	-24.21	...	...	0.20	...	2, 4	[11.09, 11.33]	1.12
PG 1613+658	0.129	?	NICMOS	H	-25.83	-25.91	...	...	0.14	...	5	11.64	2.02
PG 1617+175	0.112	?	NICMOS	H	-23.34	-25.40	...	...	0.01	...	5	10.65	0.13
PG 1626+554	0.133	E	NICMOS	H	-24.27	-25.29	...	...	0.20	5.53	5	11.02	-0.09
PG 1700+518	0.292	?	NICMOS	H	-25.64	-27.85	...	...	0.08	...	5	11.57	2.07
PG 1704+608	0.372	S	WFPC2	V	-23.86	-25.43	...	...	0.20	...	2, 4	11.70	2.08

TABLE 1 — *Continued*

Name (1)	z (2)	Morp. (3)	Inst. (4)	Band (5)	$M_{\rm host}$ (6)	$M_{\rm nuc}$ (7)	$m_{\rm total}$ (8)	host fraction (9)	$\sigma_{\rm host}$ (10)	R_e (kpc) (11)	Ref. (12)	log M$_\star$ ($M_\odot$) (13)	log SFR ($M_\odot$ yr^{-1}) (14)
		...	NICMOS	J	...	...	14.08	0.250	0.22	...	6		
		...	NICMOS	H	...	...	13.40	0.217	0.22	...	6		
		...	NICMOS	K	...	...	12.39	0.140	0.22	...	6		
PG 2130+099	0.063	B+D	NICMOS	H	-24.29	-25.02	...	...	0.23	2.83	5	11.03	0.46
PG 2214+139	0.066	E	NICMOS	H	-24.61	-24.49	...	...	0.14	2.78	5	11.16	-0.01
PG 2233+134	0.325	D	NICMOS	H	-24.19	-25.89	...	...	0.22	...	1	10.99	1.78
PG 2251+113	0.326	?	NICMOS	H	-24.79	-27.74	...	...	0.01	...	5	11.23	1.67
PG 2349–014	0.174	?	NICMOS	H	-25.88	-26.35	...	...	0.05	...	5	11.66	...
2M J005055.7+293328	0.136	S	WFPC2	I	-22.45	-20.45	...	...	1.00	...	3	[10.82, 11.05]	1.20
2M J015721.0+171248	0.213	?	WFPC2	I	-22.05	-20.85	...	...	1.00	...	3	[10.66, 10.89]	1.77
2M J023430.6+243835	0.310	...	WFPC2	I	-23.25	-24.05	...	...	1.00	...	3	[11.14, 11.37]	...
2M J034857.6+125547	0.210	?	WFPC2	I	-22.25	-19.55	...	...	1.00	...	3	[10.74, 10.97]	1.84
2M J125807.4+232921	0.259	?	WFPC2	I	-22.45	-23.75	...	...	1.00	...	3	[10,82, 11.05]	1.63
2M J130700.6+233805	0.275	E	WFPC2	I	-22.85	-18.95	...	...	1.00	...	3	[10.98, 11.21]	2.37
2M J145331.5+135358	0.139	S	WFPC2	I	-22.85	-19.65	...	...	1.00	...	3	[10.98, 11.21]	1.82
2M J163700.2+222114	0.211	S	WFPC2	I	-23.15	-21.65	...	...	1.00	...	3	[11.10, 11.33]	1.54
2M J165939.7+183436	0.170	?	WFPC2	I	-22.85	-22.45	...	...	1.00	...	3	[10.98, 11.21]	1.60
2M J171442.7+260248	0.163	S	WFPC2	I	-22.85	-22.45	...	...	1.00	...	3	[10.98, 11.21]	0.64
2M J222221.1+195947	0.211	?	WFPC2	I	-22.75	-23.35	...	...	1.00	...	3	[10.94, 11.17]	1.29
2M J222554.2+195837	0.147	S	WFPC2	I	-23.35	-17.95	...	...	1.00	...	3	[11.18, 11.41]	1.33
2M J234449.5+122143	0.199	...	WFPC2	I	-23.15	-23.45	...	...	1.00	...	3	[11.10, 11.33]	1.53

NOTE. — Column (1): the name of the quasars; Column (2): redshift; Column (3): morphology (E = Elliptical, S = Spiral, B+D = Bulge+Disk, Dp = Disk present, ? = Ambiguous); Column (4): the instrument used for HST observations, and $\star$ for ground-based AO observations; Column (5): magnitudes bands; Column (6): the absolute magnitudes of the host galaxies; Column (7): the absolute magnitude of the nuclei. Note both Column (6) and (7) have been rescaled into the same cosmology, i.e. H_0 = 70 km s^{-1} Mpc $^{-1}$, $\Omega_M = 0.3$ and $\Omega_\Lambda = 0.7$; Column (8): total apparent magnitudes; Column (9): the host fraction; Column (11): photometric uncertainty of host magnitudes; Column (11): the effective radius; Column (12): references, 1.McLeod & McLeod (2001); 2. Hamilton et al. (2002); 3. Marble et al. (2003); 4. Hamilton et al. (2008); 5. Veilleux et al. (2009); 6. Shang et al. (2011); 7. Guyon et al. (2006); Column (13): stellar masses calculated in this paper, the ones with two values are derived from optical photometry with two mass-to-light ratios (see text); Column (14): SFR from Shi et al. (2014).